Experimental Thermal and Fluid Science 109 (2019) 109851

Contents lists available at ScienceDirect

Experimental Thermal and Fluid Science

journal homepage: www.elsevier.com/locate/etfs

Impact of sensor housing geometries on transient stagnation pressure measurements in impulse facilities

Zhaoguang Wang*, Marcus Giglmaier, Thomas Hopfes, Lea Köglmeier, Nikolaus A. Adams

Institute of Aerodynamics and Fluid Mechanics, Technical University of Munich, 85748 Garching, Germany

A B S T R A C T

The measurement of transient stagnation pressure in impulse facilities, such as shock tubes and expansion tubes, is critical due to the limited experimental time window. In the present study, we investigate the characteristic behavior of pressure sensors shielded by blunt and conical housings, and evaluate the specific influence of the housing dimensions on the stagnation pressure measurement in distinct flow conditions. Pressure signals of piezoelectric sensors were acquired and schlieren images visualizing the wave dynamics were recorded. We conducted additional numerical simulations to support our hypotheses concerning the flow inside the housings. Results indicate that the pressure signal for conical housings exhibits longer rise time and more pronounced oscillations compared to that for blunt housings. Enlarging the borehole diameter and reducing the cavity depth both shorten signal rise time but enhance overshoots. Additional experiments on the sensitivity to assembly misalignment, the effect of gelatin-filled housings and the performance of exposed sensors complete the study.

1. Introduction

Pitot tubes have been widely adopted for total pressure measurements due to the low cost and the simplicity of operation. The measured pitot pressure is normally used to derive the flow velocity or the volumetric flow rate in steady/quasi-steady flows [1,2].

For subsonic flows, the Pitot tube directly measures the flow total pressure $p_{0\infty}$ with the presumption of isentropic deceleration, where

$$p_{0\infty} = p_\infty \cdot \left(1 + \frac{\kappa - 1}{2} M_\infty^2\right)^{\frac{\kappa}{\kappa-1}} \tag{1}$$

with p_∞, M_∞ and κ being the freestream static pressure, the Mach number and the heat capacity ratio, respectively. However, more complexities are added when the flow reaches supersonic conditions. The deceleration of supersonic flows to stagnation conditions typically involves the formation of shocks [3] and hence, total pressure losses. To take them into account, the center of the detached bow shock ahead of the Pitot tube is assumed to fulfill the normal shock relations. Then, the static pressure ratio across the shock $\bar{p}/p_\infty$ and the post-shock Mach number $\bar{M}$ are solely dependent on the pre-shock Mach number M_∞ and the gas heat capacity ratio κ [4]:

$$\bar{p} = p_\infty \cdot \left(1 + \frac{2\kappa}{\kappa + 1}(M_\infty^2 - 1)\right) \tag{2}$$

$$\bar{M}^2 = \left(1 + \frac{\kappa - 1}{2} M_\infty^2\right)\left(\kappa M_\infty^2 - \frac{\kappa - 1}{2}\right)^{-1} \tag{3}$$

By assuming that there is again an isentropic flow behind the shock, both the pre- and the post-shock quantities satisfy Eq. (1) individually. Hence, the Pitot tube measures the post-shock stagnation pressure $\bar{p}_0$, and the stagnation pressure $p_{0\infty}$ of the pre-shock undisturbed flow is deduced as:

$$p_{0\infty} = \bar{p}_0 \cdot \left(\frac{2\kappa M_\infty^2 - (\kappa - 1)}{\kappa + 1}\right)^{\frac{1}{\kappa-1}} \left(\frac{(\kappa - 1) + 2/M_\infty^2}{\kappa + 1}\right)^{\frac{\kappa}{\kappa-1}} \tag{4}$$

Folsom [5] and Chue [6] provided comprehensive reviews of the Pitot tube technique, and summarized various tube designs and calibration methods. However, the response rate of conventional Pitot tubes is too low for the transient pressure measurement in impulse facilities.

In shock tubes or expansion tubes where the experimental time tends to be extremely short, piezoelectric or piezoresistive pressure sensors are preferred due to their short response time and high resonant frequency paired with the high sensitivity to even small pressure fluctuations [7–9]. These sensors are positioned towards the freestream, creating a stagnation area at the tip and measuring the flow stagnation pressure on the same principle as conventional Pitot tubes. Housings that surround the sensors are used to protect them from being damaged by the fast-travelling fragments of metal diaphragms [10–14]. Such shielding designs normally leave a narrow borehole and a shallow cavity connecting the sensor surface to the ambient flow, as the two typical geometries shown in Fig. 1.

Housings with conical tips have been commonly employed in conventional pressure measurements [6,15,16]. One advantage is the less influence on the far-field flow than blunt tips. In supersonic flows where

* Corresponding author.
E-mail address: zg.wang@tum.de (Z. Wang).

https://doi.org/10.1016/j.expthermflusci.2019.109851
Received 25 January 2019; Received in revised form 24 May 2019; Accepted 15 June 2019
Available online 29 June 2019

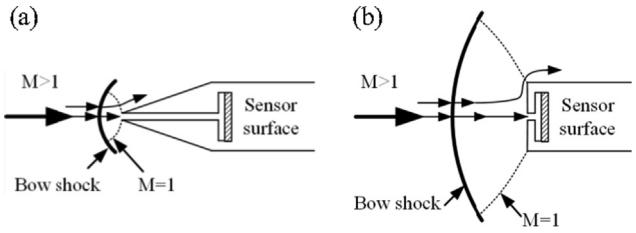

Fig. 1. Flow structures around a conical housing (a) and a blunt housing (b) in supersonic flows.

detached bow shocks are present in front of the housings, the stand-off distance is shorter for the conical tip. This would suggest less interaction of the shock with the freestream and hence, weaker effects on the downstream setup. Another advantage is that the smaller subsonic area behind the bow shock makes the conical tip less likely to be influenced by the surrounding disturbance. This would improve the measurement accuracy and consistency.

However, limited by the exterior geometry, the conical housing naturally results in a longer internal borehole than the blunt housing. Consequently, in transient pressure measurements, the wave propagation inside the conical housing would take longer time. The temporal response of the resulting pressure signal might be retarded correspondingly. In addition, at the abutting surface of the conical tip, the flow directly accelerates from the stagnation point in the center to Mach number $M = 1$ at the periphery. The area-averaged pressure over the cross section would differ from the stagnation pressure. The comparatively high curvature of the bow shock for the conical housing, which challenges the previous assumption of normal shock relations, might cause further inaccuracy to the calculation of the freestream stagnation pressure.

The present study attempts to make a thorough comparison between the conical and the blunt housings in terms of the performance in transient stagnation pressure measurements. The results would serve as general guidance on sensor housing designs.

2. Methods

2.1. Experiments

The current experimental research was carried out in a shock tube. As depicted in Fig. 2, the shock tube is composed of a driver section (3 m), a driven section (19.5 m) and a test section (0.5 m) attached to the end. The inner cross section has a diameter of 290 mm and changes to a square with the side length of 190 mm through a cookie-cutter in front of the test section. A diaphragm, which initially separates the driver and driven sections, ruptures as a critical pressure difference is reached. Subsequently, a shock wave develops and propagates towards the downstream test section and entails a flow of uniform pressure and

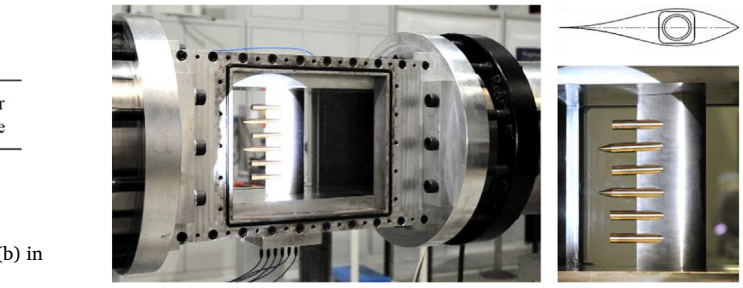

Fig. 3. Experimental Pitot rack for the stagnation pressure measurement in the test section. The incident shock arrives from left.

velocity.

In terms of the measurement system, pressure gauges and K-type thermocouples measured the initial experimental conditions at the driver and driven sections, and a NI™ cDAQ device collected the signals. Four PCB Piezotronics ICP® fast-response pressure sensors were flush-mounted along the driven section to monitor the propagation of the shock wave. An LTT device recorded the pressure data at a sampling rate of 1 MHz to determine the shock speed accurately. For visualization of the flow field inside the test section, a Z-type schlieren system was employed. A 150 W Xenon lamp served as the light source and a Shimadzu HyperVision HPV-X ultra-high-speed camera recorded 128 consecutive images of 250 × 400 pixels at a framing rate of 200 kfps. The resultant schlieren photographs have a resolution of 0.175 mm/pixel.

The stagnation pressure behind the incident shock wave was measured by a rack of Pitot probes in the test section, which were positioned opposite to the incoming flow as depicted in Fig. 3. The rack was built based on a modified Guderley profile to weaken the interaction with the incident shock wave and to avoid the formation of new shocks. A maximum number of six probes could be mounted on the rack and the interaction between them was experimentally verified to be negligible. From top to bottom, the second and the third slots for the probes were manufactured with a 2° downward inclination to investigate the sensitivity of the pressure measurement to the assembly misalignment.

Each Pitot probe on the rack was equipped with a PCB Piezotronics ICP® fast-response pressure transducer (Model 113B21) with a resonant frequency above 500 kHz and a rise time below 1 μs. The sensors were mounted in either conical or blunt housings, of which detailed geometries and dimensions are displayed in Fig. 4.

The conical housing has a 15° sloped surface relative to the centerline, resulting in a significantly longer borehole ($L = 3.11$) than the blunt housing ($L = 0.23$). The borehole diameter D varies among 0.36 (default), 0.45 and 0.54 and the cavity depth G ranges over 0.045 (default), 0.12 and 0.19. These two parameters were investigated separately.

The experiments were conducted under three distinct flow

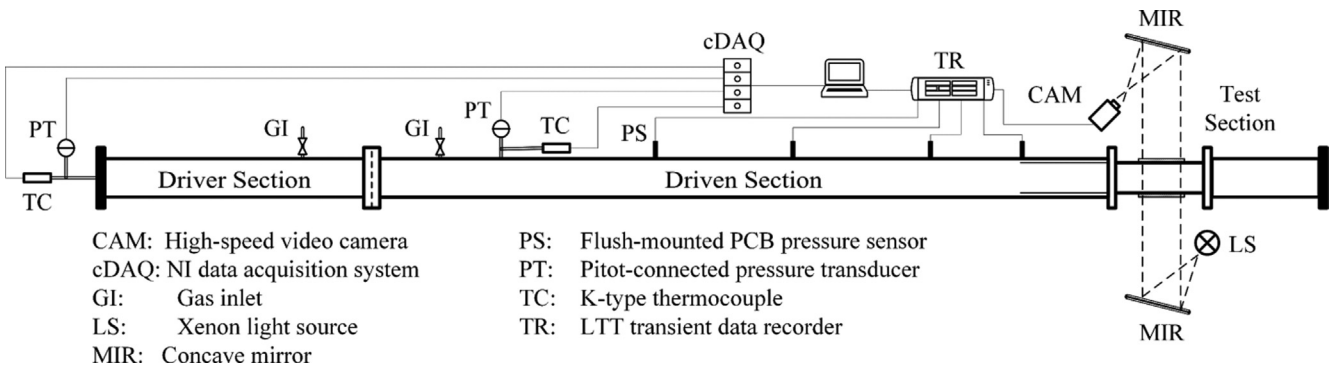

Fig. 2. Layout of the shock tube and the associated measurement system.

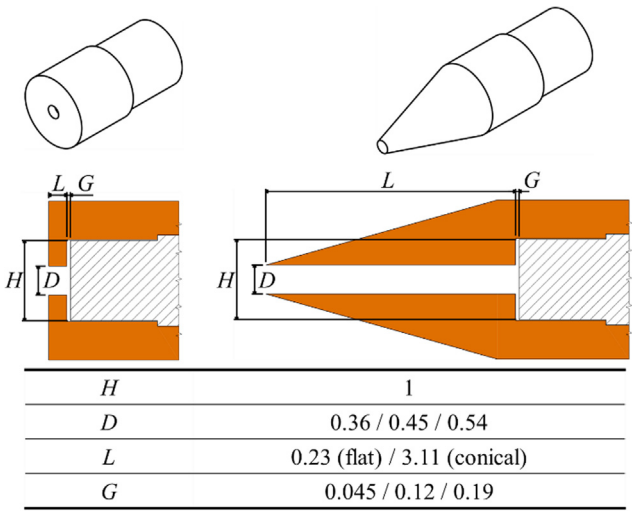

H	1
D	0.36 / 0.45 / 0.54
L	0.23 (flat) / 3.11 (conical)
G	0.045 / 0.12 / 0.19

Fig. 4. Dimensions of blunt and conical housings (orange colored) normalized by the sensor tip diameter h = 5.54 mm. The shadowed regions represent the pressure sensors. (For interpretation of the references to colour in this figure legend, the reader is referred to the web version of this article.)

Table 1
Experimental flow conditions for the stagnation pressure measurement.

$PR = p_4/p_1$		10 (± 3%)	100 (± 2%)	1000 (± 5%)
Theoretical	M_s	1.61	2.37	3.15
	M_∞	0.70	1.15	1.40
Experimental	M_s	1.50	2.24	3.01
	$\boldsymbol{M_\infty}$	**0.60**	**1.08**	**1.36**
	u_∞	241 m/s	518 m/s	775 m/s
	$Re_{\infty,D}$	25,000	4800	700

conditions as listed in Table 1. The driver and driven sections are filled with air to pressures p_4 and p_1, respectively. The pressure ratio (PR) between them is varied by keeping p_4 around 7 bar while reducing p_1, and controlled at 10, 100, and 1000, corresponding to subsonic, transonic and supersonic flow conditions in the test section. In the table, M_s, M_∞, u_∞ and $Re_{\infty,D}$ are the Mach number of the incident shock, the Mach number of the post-shock freestream flow, the freestream velocity and the Reynolds number based on u_∞ and the default housing borehole diameter D = 0.36 (2 mm).

The experimental shock speed u_s was measured by monitoring the time lag between two pressure sensors mounted shortly upstream of the test section. Thus, M_s was obtained through dividing u_s by the speed of sound calculated from the driven gas temperature. Then, M_∞ and u_∞ were derived from the moving shock relations. The increased flow Mach number goes along with a decreased Reynolds number since the reduction of the flow density outweighs the increase in the flow speed.

2.2. CFD

In order to support understandings from the experiments, numerical simulations were carried out. The commercial CFD solver ANSYS FLUENT 19.1 was employed to solve a transient, compressible, two-dimensional and axisymmetric flow field. Appropriate initial and boundary conditions were assigned according to the experiments listed in Table 1. The interior and exterior surfaces of the housing were treated as no-slip walls with a fixed temperature. Air was modeled as ideal gas. For the case of PR = 1000, the laminar viscous model was used, while the k-ω SST turbulence model was chosen for the other two higher-Re cases.

A sufficient structured mesh with a total number of 100,000 cells was applied. In order to resolve the wall bounded flow accurately, the dimensionless wall distance y^+ was kept around one.

3. Results and discussion

To assess the measurement accuracy, the pressure signal p is normalized by the expected pressure p_{ref}, which equals to the freestream total pressure $p_{0\infty}$ for subsonic flows and the post-bow shock total pressure $\bar{p}_0$ for supersonic flows. In the present experiments, the static pressure of the freestream p_∞ behind the incident shock is first derived from measured p_1 and M_s based on the moving shock relations. The value of p_{ref} is further obtained by calculating $p_{0\infty}$ from Eq. (1) or $\bar{p}_0$ from Eq. (4). The normalized pressure P is defined as:

$$P = (p - p_1)/(p_{ref} - p_1) \tag{5}$$

with P = 0 representing the initial pressure and P = 1 the expected stagnation pressure. Since the normalization is based on the case-specific shock strength, the influence of the slight PR variation under each flow condition is negligible.

Pressure signals measured by sensors with different housing configurations are presented in this section. Main signal features are discussed with the help of schlieren images and simulation results. Section 3.1 shows the general flow wave motions surrounding the housings. Distinct signal characteristics for each housing geometry are presented in Section 3.2. The behavior of housings at different flow March numbers is presented in Section 3.3. Effects of varying the borehole diameter and the cavity depth are discussed in Sections 3.4 and 3.5, respectively. With the preceding two sections focused on the assembly misalignment and the gelatin-filled housings, Section 3.8 wraps up the discussion by evaluating the performance of exposed sensors.

3.1. Wave dynamics around the housings

Wave dynamics in the freestream around housings is discussed with schlieren images. The associated wave motions are mainly determined by the exterior geometry of the housings, and the interior void plays a supplementary role. The wave evolution determines when the flow outside the housings becomes steady, which further influences the settling time of the measured pressure signals to a certain extent.

Fig. 5 displays the schlieren images for the blunt housing under different pressure ratios. Only the top half of the geometries are provided owing to the symmetry. For each flow condition, the left column is the first image after the impact of the incident shock on the housing and is referred as time t_0. Shock reflection occurs at the housing front, and the reflected shock travels in the upstream direction and expands radially. According to theory, the speed of the reflected shock decreases with increasing the flow Mach number as seen in the second column. At time t_0 + 360 μs for the subsonic flow, intense separation is observed covering the entire outer surface of the housing. Meanwhile, the reflected shock disintegrates by traveling upstream. In contrast, the reflected shock is stabilized at a certain position for the transonic and supersonic cases as detached bow shocks. During the process, there are other waves developing around the housing exteriors. But they tend to be isolated from the upstream housing tips by supersonic regions in between and hence, exert little effects on the pressure measurement.

Fig. 6 shows the schlieren images for the conical housing. The flow fields exhibit certain resemblance to those in Fig. 5. In the first column, the incident shock is reflected at the housing tip and the sloped surface. The resulting reflected shock is substantially weaker than that for the blunt housing. For the supersonic flow, there is barely any reflection observable, as the flow density is considerably low making the schlieren phenomena less effectual. Shock positions in the second column show that, the reflected shock propagates upstream at a much lower velocity than cases with the blunt housing. For the two cases with $M_\infty > 1$, the reflected shock gradually settles down as a detached bow shock, similarly to the observations in Fig. 5. But as shown in the third column, the stand-off distance is relatively small and the shock profile is strongly

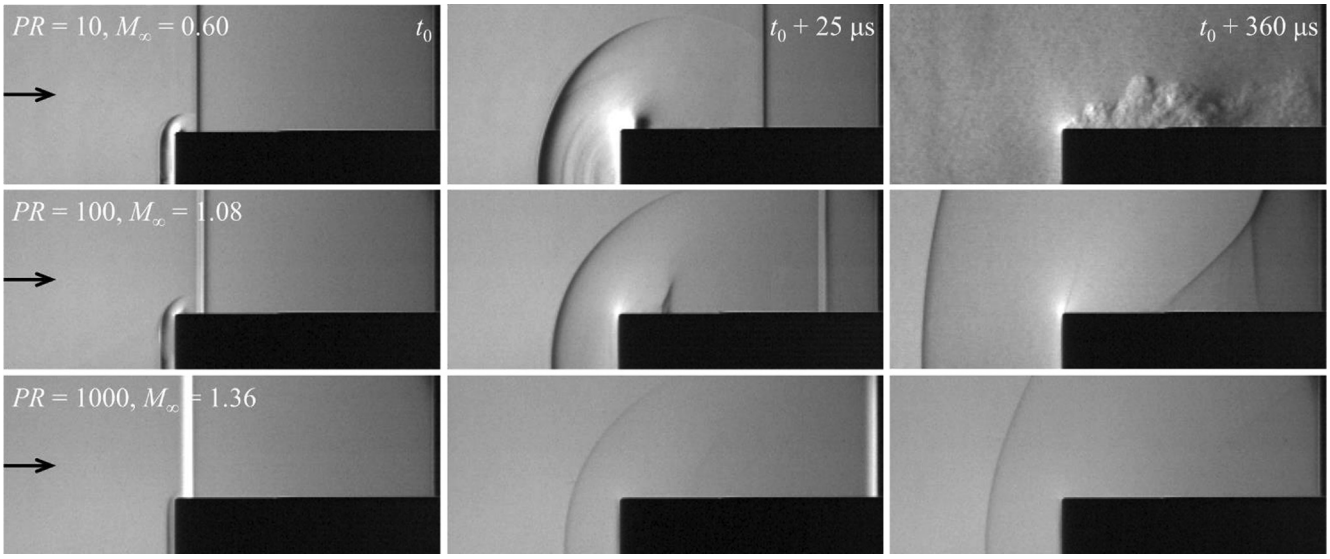

Fig. 5. Schlieren images of the flow field around the upper half of the sensor with the blunt housing. The incident shock and the induced freestream flow propagate from left to right. Each row corresponds to a certain flow Mach number, while each column to a specified time moment.

curved.

From the viewpoint of shock structures, the less-curved bow shock for the blunt housing satisfies the presumption of normal shock relations better. Hence, the blunt housing is expected to give more accurate pressure measurements. As to the duration of the transient wave motions, it is difficult to determine the exact moments for the waves to become stabilized. But a general trend is that the wave settling time declines as the flow velocity increases.

3.2. Characteristic pressure signals

Pressure signals measured by sensors with blunt and conical housings under identical flow conditions are compared in this section. The signal characteristics are closely related to the flow evolution inside the housings. The analyses of wave motions in Schlieren images accompanied with the simulation results provide insight into the internal flow features. In following figures, the experimental time t is regarded as zero at the initiation of the signal rise.

Fig. 7 shows the pressure signals measured with blunt and conical housings at $PR = 100$ for a comparison of respective signal features.

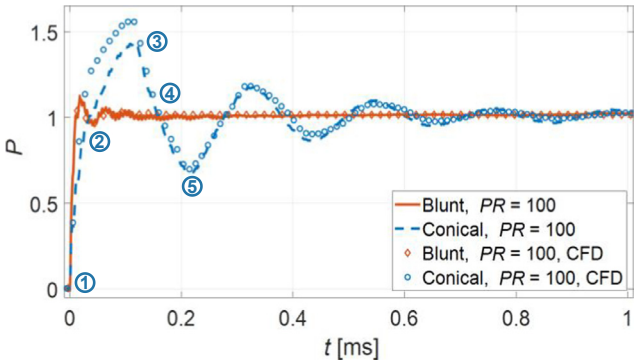

Fig. 7. Normalized pressure signals for blunt and conical housings ($D = 0.36$, $G = 0.045$) at $PR = 100$.

The signal for the sensor shielded by the blunt housing surges upwards at the beginning and exhibits a weak overshoot. The pressure soon becomes stabilized at the expected value after a short period of weak oscillations. In contrast, the signal for the conical housing rises slowly

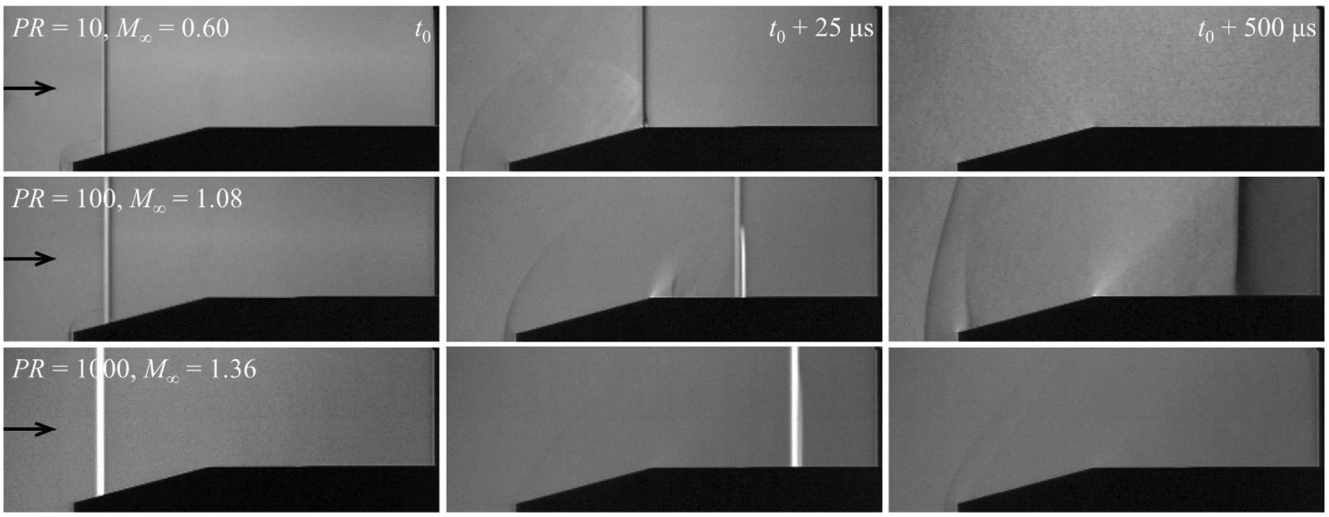

Fig. 6. Schlieren images of the flow field around the upper half of the sensor with the conical housing. The incident shock and the induced freestream flow propagate from left to right. Each row corresponds to a certain flow Mach number, while each column to a specified time moment.

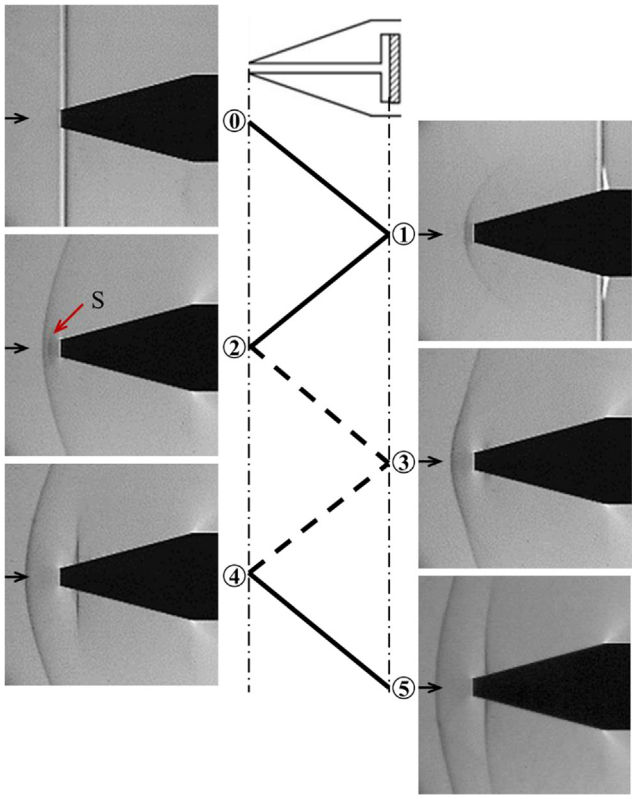

Fig. 8. Sketch of the wave dynamics inside the conical housing and schlieren images of the wave motions outside. Solid lines represent shock waves, and dashed lines expansion waves.

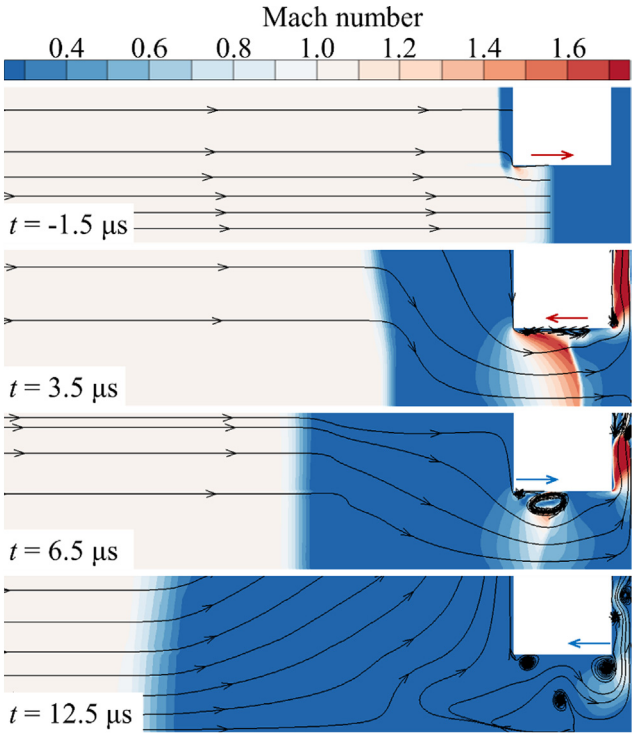

Fig. 9. Mach number contours with arrowed streamlines in the borehole for the blunt housing at $PR = 100$. The red and the blue arrows indicate the moving directions of the shock and the expansion waves, respectively. (For interpretation of the references to colour in this figure legend, the reader is referred to the web version of this article.)

to the reference value and reaches a strong overshoot. Through a long lasting of large-amplitude oscillations, the signal gradually settles down around the expected value.

The strong oscillations for the conical housing arise from the wave motions inside the housing void. A sketch of the speculated wave dynamics in the borehole is displayed in Fig. 8. Schlieren images at specified time moments are also provided to present external flow fields. The plotted solid lines represent shock waves and the dashed lines expansion waves. The numeric labels correspond to the time moments in Fig. 7.

When the incident shock impacts on the housing tip, part of the shock propagates into the borehole/cavity and entails a flow behind. At the time moment ①, this shock gets reflected at the sensor surface and causes the pressure signal to start rising. The reflected shock travels upstream, and meets the external freestream at the borehole inlet. A weak shock, which is labelled as "S" in the schlieren image ②, is emitted from the housing tip towards the detached bow shock. Meanwhile, since the gas inside the borehole is over-compressed by the incident shock and the succeeding reflected shock, an expansion wave travels from the borehole inlet inwards and reduces the flow pressure. The pressure signal begins to drop when the expansion wave arrives at the sensor tip at ③. The subsequent reflected expansion wave over-expands the flow, decreasing the flow pressure below the reference value. At ④, this reflected expansion wave reaches the housing tip and interacts with the external flow, releasing a new shock into the borehole. As this shock arrives at the sensor tip at ⑤, the pressure signal is re-boosted and one cycle of the oscillations is completed. One point of interest is that during this process, the detached bow shock moves back and forth slightly, at a synchronized pace with the pressure oscillations. The wave dynamics inside the blunt housing occurs in a similar pattern, but at a much faster rate due to the significantly shorter borehole length.

Although supported by the schlieren images, the wave motions sketched in Fig. 8 are oversimplified. Effects of viscous dissipation, heat transfer and flow mixing are still to be revealed. Hence, the simulation results are also presented here to verify the main ideas delivered in Fig. 8 and supplement further details. The pressure signals obtained from the numerical simulations are also included in Fig. 7 for validation. The experimental and the numerical results match reasonably well, with certain discrepancies in the signal overshoot which could be caused by the simplified isothermal boundary conditions imposed on the housing surfaces.

Fig. 9 presents the Mach number contours with arrowed streamlines inside the blunt housing at $PR = 100$. Only the upper half of the cross section is displayed due to the symmetry. The contours at $t = -1.5\,\mu s$ clearly show that part of the incident shock propagates into the borehole. At $t = 3.5\,\mu s$ after the shock gets reflected, the post-shock high-pressure region serves as a reservoir to fill the cavity in front of the sensor tip. The flow chokes around the cavity corner under the high pressure ratio. At $t = 6.5\,\mu s$ the newly developed expansion wave departs from the borehole inlet and arrives at the sensor tip at $t = 12.5\,\mu s$. Then the choking behavior disappears and the filling of the cavity is interrupted. Indicated by the streamlines at the housing front, there is no more flow into the borehole at this time moment, and the pressure measured by the sensor starts to drop.

The Mach number contours inside the conical housing at $PR = 100$ are shown in Fig. 10, of which the left column corresponds to the region near the housing tip and the right column in front of the sensor surface. Similar behavior, such as the reflection of the incident shock at the sensor surface and the propagation of the new expansion wave into the borehole, is present. But as expected, the corresponding time period is largely elongated. A choking throat also appears at the corner during the cavity filling process ($t = 5\,\mu s$). At $t = 78\,\mu s$ before the arrival of the expansion wave (which can be identified at $t = 110\,\mu s$ by the change of the flow direction), the choking phenomenon already vanishes, indicating that the cavity has been filled up to a relatively high pressure level.

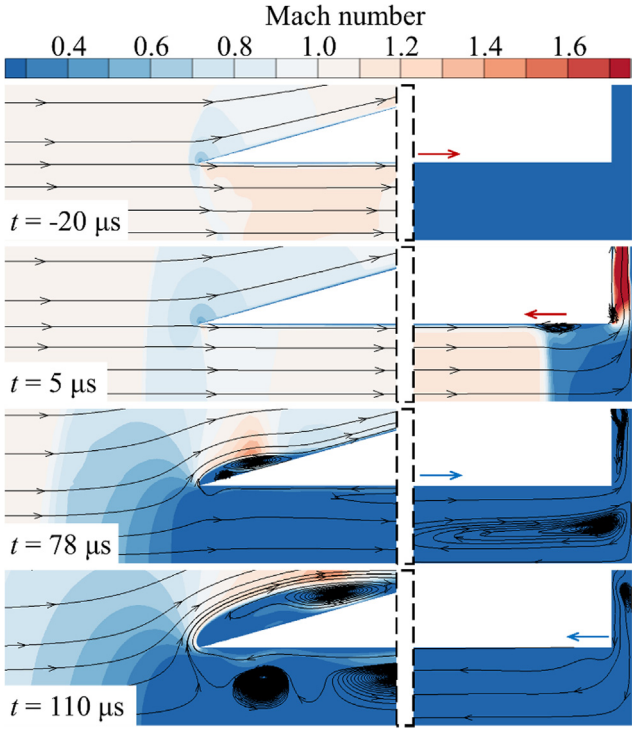

Fig. 10. Mach number contours with arrowed streamlines near the borehole inlet (left) and near the sensor tip (right) for the conical housing at $PR = 100$. The red and the blue arrows indicate the moving directions of the shock and the expansion waves, respectively. (For interpretation of the references to colour in this figure legend, the reader is referred to the web version of this article.)

The simulation results generally agree well with the hypothetical wave dynamics inside the housings presented in Fig. 8. Some details such as the choking behavior in the cavity are supplemented in Figs. 9 and 10. With this understanding, specific properties of the pressure signals shown in Fig. 7 are analyzed individually as follows.

The rise time, which is traditionally defined as the time period for the signal to rise from 10% to 90% of the steady value, is mainly determined by the initial mass flow rate of the cavity filling. A higher mass flow rate consumes less time to fill the cavity up to the reference pressure, meaning a shorter rise time. As indicated in Fig. 9 ($t = 3.5$ μs) and Fig. 10 ($t = 5$ μs), the flow is choked around the cavity corner at the beginning of the filling process for both blunt and conical housings. Then the filling mass flow rate solely depends on the total pressure of the flow ahead of the choking throat, considering the choking area is the same. Fig. 11 compares the total pressure distribution inside the borehole between the two housing designs at respective filling moments. The total pressure p_0 is normalized by the expected reference pressure p_{ref}. For the blunt housing, the total pressure is raised noticeably above p_{ref}, since the reflected shock in front of the housing is moving against the incoming flow. However, for the conical housing, the frontal reflected shock is rather weak and exerts little effects on the flow total pressure ($p_0/p_{ref} \sim 1$). As a result, the filling mass flow rate for the conical housing is relatively low and the rise time is comparatively long.

The maximum overshoot represents the peak value of the signal. The overshoot behavior is caused by the reflection of the incident shock inside the housing void, which over-compresses the flow and tends to fill the cavity to the pressure higher than p_{ref}. For the blunt housing, the filling process is interrupted by the arrival of the expansion wave at the sensor surface as illustrated in Fig. 9 ($t = 12.5$ μs). Hence, the maximum overshoot is suppressed at a low level. However, the conical housing experiences a fairly complete filling process and the resulting overshoot is much stronger.

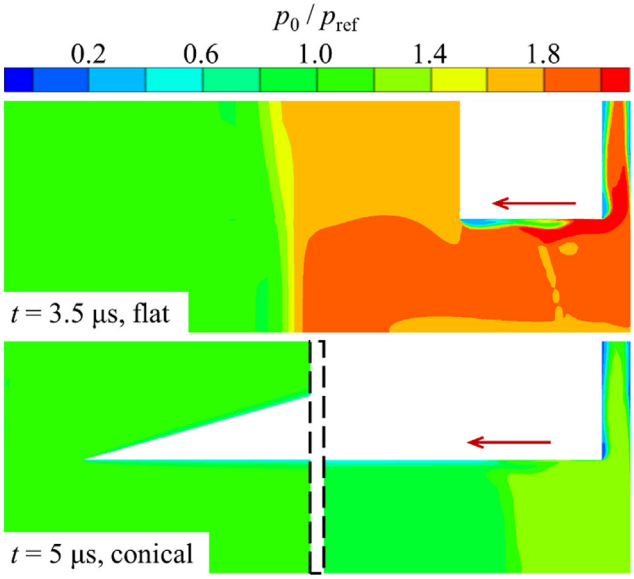

Fig. 11. Normalized total pressure contours inside the borehole for the blunt (top) and the conical (bottom) housings at $PR = 100$.

The oscillation frequency of the signal is dominated by the wave propagation inside the housing void as previously explained. For experiments under the same flow condition, the wave travelling speeds tend to remain similar, with limited variations caused by changes in the housing geometries or dimensions. Then the borehole length plays the decisive role to determine the oscillation period. The conical housing, which has a significantly longer borehole, naturally yields a much lower oscillation frequency.

The settling time, defined in a conventional way as the time taken by the signal to become stabilized within the ± 5% interval of the steady value, depends on the decay rate of the oscillation amplitudes. The amplitude attenuation is partially caused by the energy exchange between the flow inside and outside of the housings through shock waves and expansion waves. Such communications drive the pressure in the housing void to reach a balance with the external freestream. Another reason for the amplitude dampening is the energy dissipation brought by viscous friction and heat transfer at the housing interior walls. Under the same flow condition ($Re_{\infty,D} = 4800$), strengths of the wall viscous stress and the wall heat flux are similar between blunt and conical housings. However, the frequent wave motions inside the blunt housing (owing to the short borehole length) efficiently exchange the pressure information with the outside freestream, restraining the cavity ahead of the sensor from being over-filled or over-drained. Comparatively, the communication between the cavity in the conical housing and the external flow field is retarded by the long borehole, resulting in a slow oscillation attenuation and a long settling time.

Overall speaking, the performance of the blunt housing is superior to the conical housing, in terms of the stagnation pressure measurements. The signal exhibits a shorter rise time, a weaker overshoot and a faster settling down.

3.3. Effect of the flow conditions

For each housing configuration, experiments are carried out under three flow conditions as listed in Table 1. The performance of blunt and conical housings in subsonic, transonic and supersonic flows are compared and discussed in this section.

Figs. 12 and 13 compare the pressure signals for blunt and conical housings at distinct flow conditions, respectively. The shadowed ribbons backgrounding each line represent the corresponding measurement uncertainty as 95% confidence intervals. The calculation is based

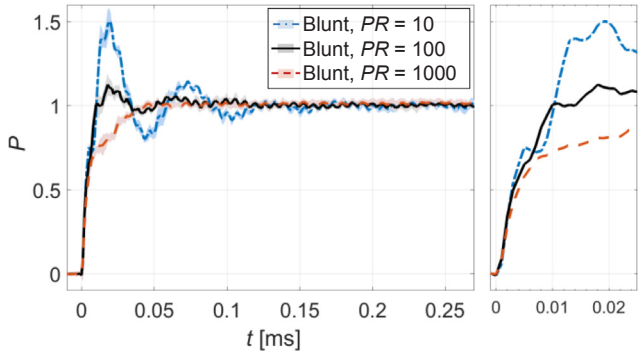

Fig. 12. Normalized pressure signals for the blunt housing ($D = 0.36$, $G = 0.045$) at different flow conditions, with the shadowed ribbons representing the measurement uncertainty. The right plot is a zoomed view of the initial pressure jump.

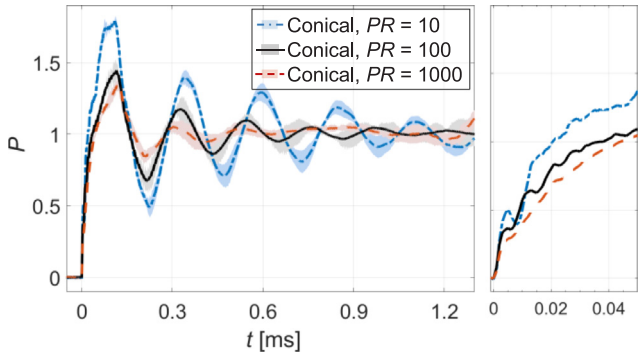

Fig. 13. Normalized pressure signals for the conical housing ($D = 0.36$, $G = 0.045$) at different flow conditions, with the shadowed ribbons representing the measurement uncertainty. The right plot is a zoomed view of the initial pressure jump.

on the *t*-distribution analyses of at least four repeated experiments. The uncertainty for blunt housings is relatively small and falls within ± 2.5%. Conical housings exhibit a higher uncertainty level, especially at the oscillation peaks and troughs where a broadest range of ± 10% is reached locally. But the characteristic signal patterns remain clearly identified. The general distinctions previously observed between blunt and conical housings are maintained at different flow conditions.

Rise times, maximum overshoots and settling times for all cases are summarized in Fig. 14. One point of notice is the drastic difference in the settling time between the two housing designs. By adopting the blunt housing, the settling time is reduced by one order of magnitude, which is of essential importance for experiments with short time windows. Another interesting point is the absence of the signal overshoot for the blunt housing at $PR = 1000$. The signal climbs slowly to the reference value and settles down immediately without further oscillations. This behavior suggests that a non-overshooting rapidly-settled signal is achievable for the stagnation pressure measurement by manipulating the sensor housing geometries.

As to the effect of the flow conditions, there appears a consistent tendency of increasing the rise time, lowering the maximum overshoot, raising the oscillation frequency and reducing the settling time as the flow changes from subsonic to supersonic conditions. These points are discussed with the help of simulation results shown in Fig. 15. Mach number contours inside the conical housing are presented at the moment when the cavity is still filling. Considering the change in the flow condition exerts similar effects on the two housing designs, only cases of the conical housing are provided.

Rise Time. As shown in Fig. 15, a separation bubble at the borehole wall appears for all flow conditions, due to the interaction of the reflected shock with the boundary layer. This separation bubble blocks

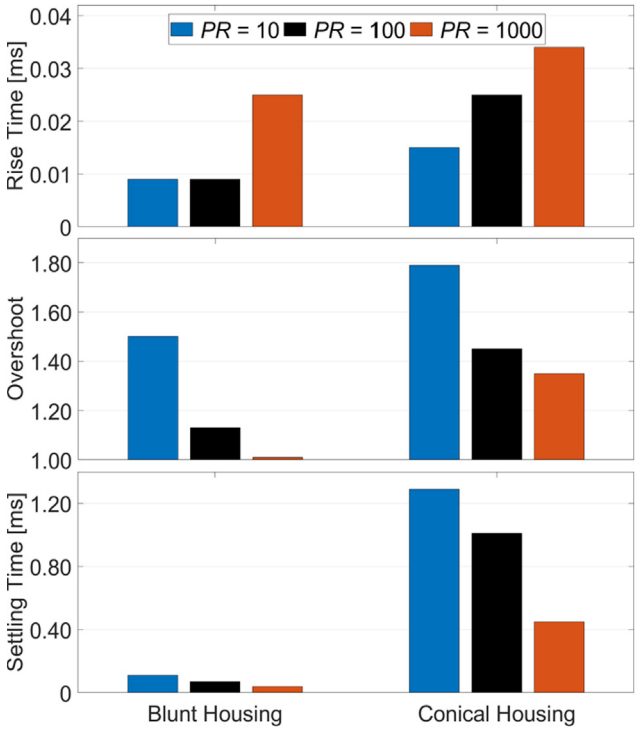

Fig. 14. Comparison of rise times (top), maximum overshoots (middle) and settling times (bottom) between blunt and conical housings at different flow conditions.

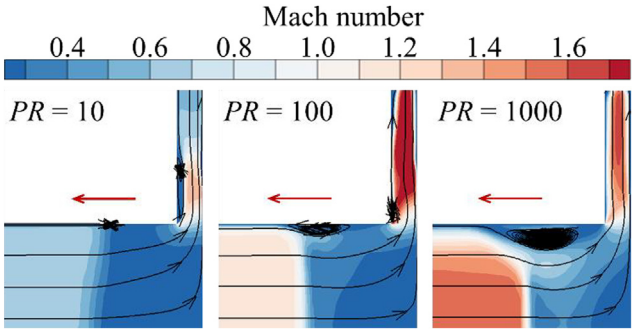

Fig. 15. Comparison of the Mach number contours in front of the sensor surface during the cavity filling process for the conical housing at different flow conditions ($t = 5\,\mu s$).

the cross section of the borehole and absorbs part of the incoming flow into the recirculation region instead of filling the downstream cavity. For cases with higher M_s and correspondingly lower $Re_{\infty,D}$, the pressure gradient across the shock is stronger and the boundary layer developed is thicker, of which both contribute to a larger separation bubble. As a consequence, the blocking effect is enhanced and the resulting rise time is extended.

Maximum Overshoot. An analytical calculation of one-dimensional shock waves shows that the reflection of the incident shock could ideally cause a maximum overshoot of 2.06, 1.89 and 1.74 for subsonic, transonic and supersonic flow conditions, respectively. Due to the filling of the cavity ahead of the sensor, the overshoots of the experimental signals are consistently lower than the theoretical values. However, this tendency of weakening the overshoot with increasing the flow Mach number is preserved.

Oscillation Frequency. Figs. 16 and 17 plot the fast Fourier transform (FFT) spectrum of the pressure signals measured for blunt and conical housings, respectively. As the flow Mach number increases from subsonic to supersonic conditions, the spectrum peaks shift towards mildly

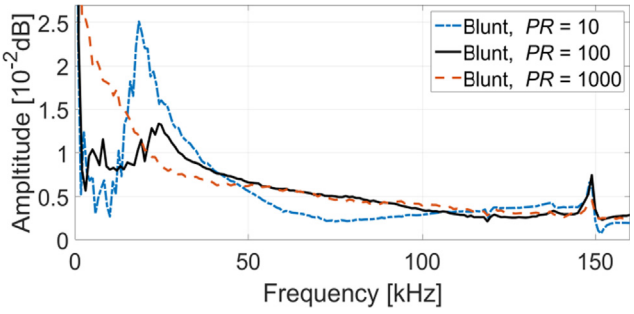

Fig. 16. FFT spectrum of the pressure signals measured for the blunt housing.

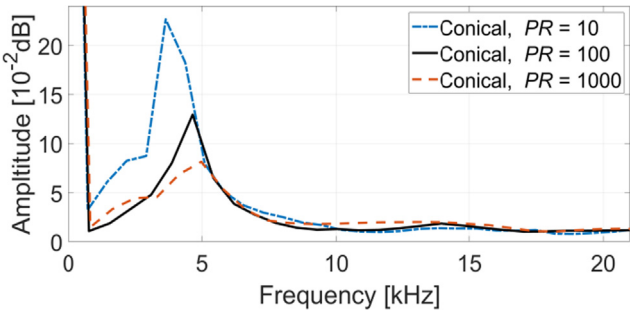

Fig. 17. FFT spectrum of the pressure signals measured for the conical housing.

higher frequencies (from 18 kHz to 24 kHz for blunt housings, and from 4 kHz to 5 kHz for conical housings). Interestingly, conical housings have boreholes 14 times longer than blunt housings, but the corresponding oscillation frequencies of the measured signals are only four to five times lower. This might be attributed to the influence of the cavity filling on the oscillation period. For the blunt housing at $PR = 1000$, no distinguishable peak exists in the spectrum, which agrees with the observation in Fig. 12 that the viscous dampening slows down the filling process and restrains signal oscillations. Peaks at the frequency 149 kHz for blunt housings correspond to the small-amplitude periodic fluctuations in Fig. 12. Conical housings exhibit similar peaks at 136 kHz, which is not presented in Fig. 17 for concision. The most likely explanation is that these high-frequency fluctuations arise from the wave motions inside the tiny gap around the lateral surface of the sensor. This gap is 6 mm long and merely 0.06 mm thick, and preserved for a smooth assembly into the housing. Since these noises exert negligible effects on the transient response of the signals, they are filtered out from the pressure data presented in following figures by a low-pass 100 kHz filter.

Settling Time. In the experiments, increasing flow Mach number is accompanied with decreasing flow Reynolds number as shown in Table 1. The lower *Re* results in stronger viscous dissipation. Increasing the flow speed also enhances the heat convection at the housing interior walls. Consequently, a stronger dampening of the oscillation amplitudes is expected for higher flow Mach numbers, and the resulting signal settling time is correspondingly shorter.

As a short summary, for experiments with higher pressure ratios, the signal overshoot is intensified and the oscillation frequency is raised due to the increasing flow Mach number. Meanwhile, the decreasing Reynolds number elongates the rise time but shortens the settling time.

3.4. Effect of the borehole diameter

Modifications of the housing interior dimensions, including the borehole diameter and the cavity depth, are examined and the associated effects on the stagnation pressure measurement are evaluated. In this section, the influence of the borehole diameter is discussed by comparing results of the housings with $D = 0.36$, 0.45 and 0.54.

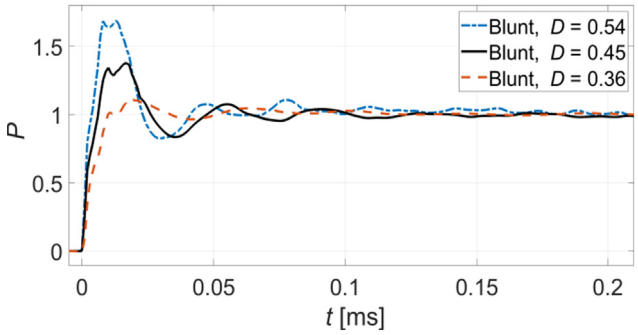

Fig. 18. Normalized pressure signals for the blunt housing ($G = 0.045$) with three different borehole diameters at $PR = 100$.

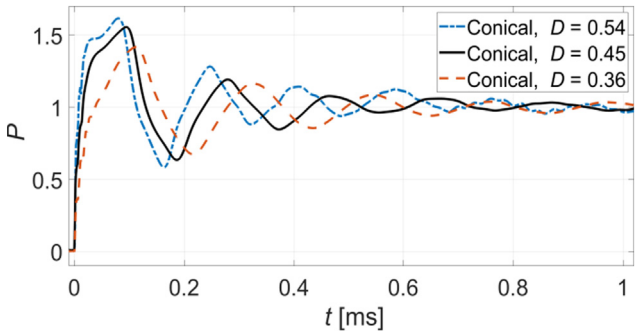

Fig. 19. Normalized pressure signals for the conical housing ($G = 0.045$) with three different borehole diameters at $PR = 100$.

The pressure signals measured by the blunt and the conical housings with different borehole diameters are presented in Figs. 18 and 19, respectively. Similar trends of the signal changes are observed for the two different housings. Larger borehole diameters bring about shorter rise times, distinctly stronger overshoots and higher-frequency oscillations. Simulation results of the Mach number and total pressure contours inside the conical housing are provided in Fig. 20 to supplement the discussion.

Rise Time. In an ideal case where no cavity exists at the end of the borehole, the reflected shock would induce a stationary field behind it. But the fact that a certain amount of flow is drawn into the cavity attenuates the strength of the reflected shock. For cases with larger borehole diameters, the amount of flow into the cavity takes up a smaller proportion of the incoming flow, thus leading to a less reduction of the reflected shock strength. This is verified in Fig. 20 where the total pressure behind the reflected shock is the highest for $D = 0.54$ and the lowest for $D = 0.36$. Consequently, the mass flow rate for the cavity filling is relatively high for housings with wide boreholes, and the respective rise times are comparatively short. The fact that the cavity volume is reduced as the borehole diameter expands, also contributes to the decreasing rise time.

Maximum Overshoot. As mentioned before, the maximum overshoot obtainable by the pressure signal is limited by the strength of the reflected shock. Although the cavity is not fully filled up to this limit, it provides reasonable indications on the overshoot strength. Since the reflected shock is enhanced by increasing the borehole diameter, a higher maximum overshoot is expected correspondingly. From Figs. 18 and 19, it is observed that the promotion of the signal overshoots as the borehole expands is more pronounced for the blunt housing. At $D = 0.54$, its maximum overshoot even overtakes that for the conical housing.

Oscillation Frequency. The enhancement of the reflected shock with increasing the borehole diameter is also reflected in higher shock speed. This can be inferred from the shock positions in Fig. 20. Consequently, the faster wave motions give rise to higher signal oscillation

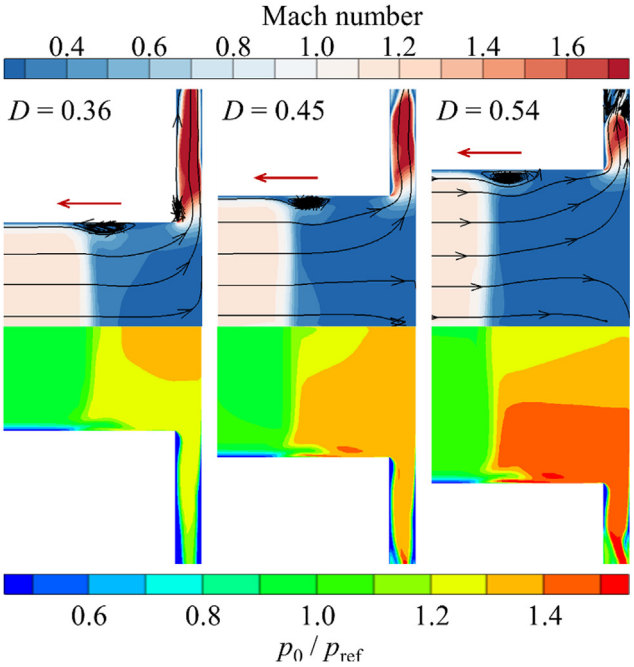

Fig. 20. Contours of the Mach number (top) and the total pressure (bottom) in front of the sensor surface during the cavity filling process for the conical housing with different borehole diameters under $PR = 100$ at $t = 5\,\mu s$.

frequencies. One point of notice is that when the borehole diameter of the conical housing is expanded, the borehole is shortened accordingly to maintain the same sloped exterior. Hence, the reduction of the borehole length is another important contributor to the increase in the oscillation frequency for conical housings.

To sum up, increasing the borehole diameter mainly works to strengthen the reflected shock, which further exerts effects on the signal rise time, the overshoot and the oscillation frequency. The signal overshoot seems particularly sensitive to the borehole diameter for the blunt housing, and a proper selection might completely remove the overshoot.

3.5. Effect of the cavity depth

This section intends to analyze the influence of the cavity depth. The experimental results for blunt and conical housings with $G = 0.045$, 0.12 and 0.19 are presented in Figs. 21 and 22, respectively.

As the cavity depth increases, the signal rise time is extended consistently while the overshoot only varies within a very limited range. For the conical housing, another noticeable change is the prolongation of the oscillation period. The simulated Mach number and total pressure contours inside the conical housing are presented in Fig. 23 for further

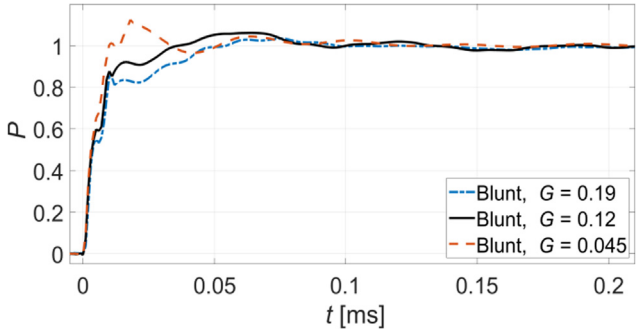

Fig. 21. Normalized pressure signals for the blunt housing ($D = 0.36$) with three different cavity depths at $PR = 100$.

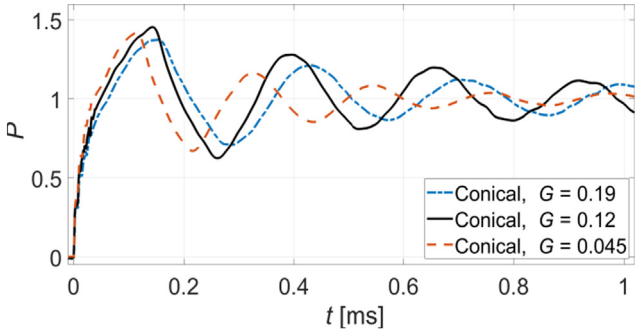

Fig. 22. Normalized pressure signals for the conical housing ($D = 0.36$) with three different cavity depths at $PR = 100$.

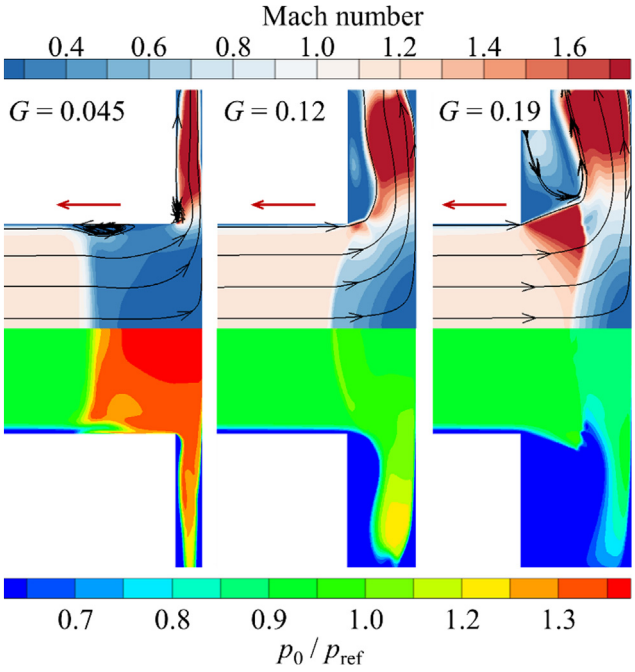

Fig. 23. Contours of the Mach number (top) and the total pressure (bottom) in front of the sensor tip during the cavity filling process for the conical housing with different cavity depths under $PR = 100$ at $t = 5\,\mu s$.

analyses.

Rise Time. For larger cavity depths, a higher proportion of the post-shock fluid is absorbed into the cavity. Correspondingly the reflected shock becomes weaker, compressing the flow to a lower pressure level as shown in Fig. 23. The simulation results present another distinct change in the flow structure. A large separation bubble is induced across the cavity corner and blocks over half of the entire cross section at $G = 0.19$. Therefore, for cases with larger cavity depths, the decreasing total pressure plus the shrinking choking area results in a less-adequate mass flow rate for the cavity filling, which accounts for the longer rise time.

Maximum Overshoot & Oscillation Frequency. Since the strength of the reflected shock decreases as the cavity depth increases, a lower overshoot is expected. The accompanied decrease in the shock velocity results in a lower oscillation frequency.

In general, increasing the cavity depth exerts opposite effects to increasing the borehole diameter. This implies that the volume ratio between the cavity and the borehole could serve as a general indicator of the housing performance.

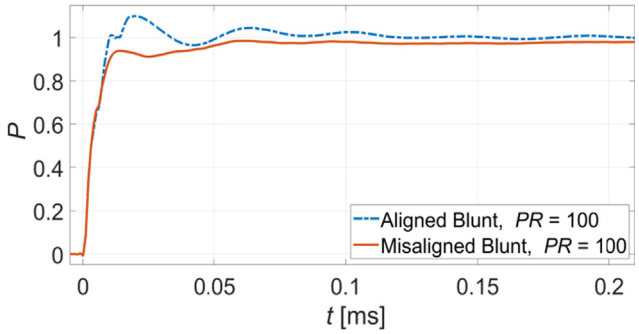

Fig. 24. Normalized pressure signals for the aligned and the 2° misaligned blunt housings (D = 0.36, G = 0.045) at PR = 100.

3.6. Effect of the assembly misalignment

One practical problem involved in pressure measurements is the misaligned mounting of sensors. To correctly measure the flow stagnation pressure, the sensor is supposed to be directed exactly opposite to the freestream flow direction. This requirement is not always satisfied, considering the assembly accuracy and the flow uniformity. Thus, evaluation of the sensitivity of the measurement setup on the mounting misalignment is necessary.

Figs. 24 and 25 present the pressure signals measured by the 2° misaligned sensors under PR = 100 for blunt and conical housings, respectively. As shown, inclining the sensor by 2° exerts negligible effects on the signal rise time and the oscillation frequency. However, a reduction is identified for the maximum overshoot, the oscillation amplitudes, and more importantly the steady value. Results of the other two flow conditions, which are not shown here for the sake of concision, have the same tendencies.

The misalignment between the housing centerline and the incoming freestream direction brings subtle changes to the housing configuration. On one hand, the effective cross section of the borehole to receive the incident shock is reduced. The resulting behavior is expected to resemble a housing with a smaller borehole. Based on the observations in Figs. 18 and 19, the reduction of the overshoot and the decrease in the oscillation amplitudes are as expected. On the other hand, the cross section of the borehole inlet is not perfectly normal to the incoming flow. Thus the presumed stagnation condition at the housing tip is not fulfilled. With only part of the flow dynamic pressure accounted for, a measurement signal lower than the stagnation pressure is expected.

Table 2 lists the steady values of the pressure signals measured in different cases. For the conical housings under PR = 10 and PR = 100, the pressure signals still exhibit a certain degree of oscillations at the end of the available experimental time. Thus the corresponding steady values are calculated as the averaged pressure over the last oscillation period. As shown in Table 2, the misaligned mounting decreases the measured pressure by a maximum of 4.08%. For both housing designs,

Table 2
Steady values of the pressure signals measured by aligned and misaligned sensors with blunt and conical housings.

Pressure ratio PR		10	100	1000
Blunt	Aligned	1.0001	1.0018	1.0037
	Misaligned	0.9807	0.9783	0.9726
	Drop	**1.92%**	**2.35%**	**3.11%**
Conical	Aligned	0.9998	0.9967	0.9933
	Misaligned	0.9674	0.9614	0.9525
	Drop	**3.26%**	**3.53%**	**4.08%**

the decrement grows as the flow Mach number increases, meaning that the supersonic flow is more sensitive to the misalignment than the subsonic flow. Under the same flow condition, the conical housing consistently gives a higher pressure reduction than the blunt one. Hence, the former design has a higher demand for the mounting accuracy.

3.7. Effect of filling the housing with gelatin

Filling the housing interior void with oil or grease is one of the methods previously proposed to accelerate the temporal response [17,18]. The idea is that the acoustic information would be delivered faster between the inside and the outside of housings due to the comparatively high sound speed in oil/grease, and the filling process would be eliminated because of the corresponding low compressibility.

To estimate the performance of this method in stagnation pressure measurements, experiments with the housing interior filled with gelatin are conducted. The gelatin is made from a mixture of distilled water, Gelrite™ Gellen gum and magnesium sulfate with the respective mass proportion of 10,000:6:5. The speed of sound in the gel is experimentally measured to be 1480 m/s. To prevent water evaporation and to avoid expansion of the tiny bubbles possibly trapped in the gelatin, only the low pressure ratio PR = 10 is studied, which corresponds to the subsonic flow condition.

Figs. 26 and 27 show the pressure signals measured for the gelatin-filled blunt and conical housings at PR = 10. With housings filled with gelatin, the signal rise time is reduced approximately to 2 μs, since the low compressibility of the filler shortens the cavity filling process significantly. Meanwhile, the overshoot is intensified noticeably, which is caused by the change in the wave motion pattern. For gelatin-filled housings, the shock wave experiences the first reflection at the air-gelatin interface, that is, at the borehole inlet. Due to the dramatic difference of the acoustic impedance between air and gelatin, this reflection happens in an almost ideal manner and increases the pressure behind the reflected shock to a level close to p_{peak}. To maintain the pressure balance across the air-gelatin interface, a compression wave is induced and propagates into the borehole. A second reflection occurs as the compression wave reaches the sensor surface and boosts the

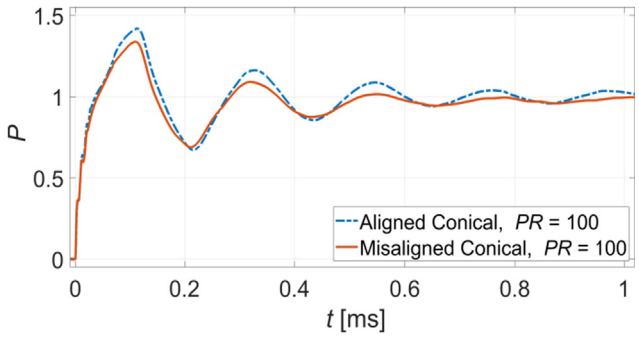

Fig. 25. Normalized pressure signals for the aligned and the 2° misaligned conical housings (D = 0.36, G = 0.045) at PR = 100.

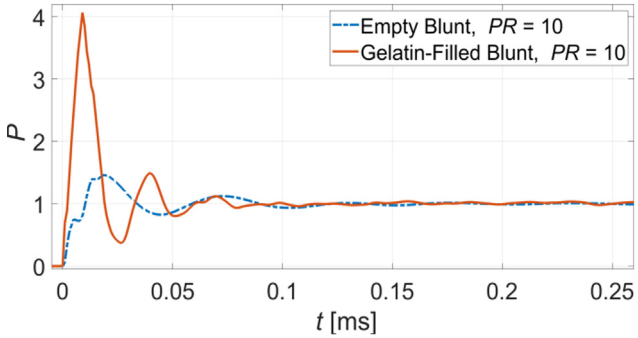

Fig. 26. Normalized pressure signals for the empty and the gelatin-filled blunt housings (D = 0.36, G = 0.045) at PR = 10.

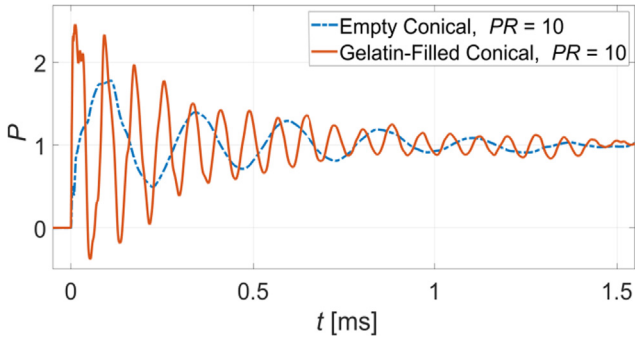

Fig. 27. Normalized pressure signals for the empty and the gelatin-filled conical housings ($D = 0.36$, $G = 0.045$) at $PR = 10$.

pressure to an even higher value, which is responsible for the stronger overshoot. In addition, the signal oscillation frequency is tripled by filling housings with gelatin, owing to the increase in the sound speed. Interestingly, the oscillation amplitudes decay almost at the same rate as cases of empty housings. Consequently, the settling time is nearly unchanged by the gelatin filling.

As noticed, the gelatin-filled blunt housing exhibits a much higher overshoot than the gelatin-filled conical one. This might be related to the strength of the reflected shock at the air-gelatin interface. For the blunt housing, the central part of the reflected shock decays comparatively slowly due to the extensive frontal surface, sending a stronger compression wave into the gelatin than the conical housing.

Overall speaking, the gelatin-filled housings exhibit no superior performance to the empty housings in the stagnation pressure measurements. Instead, the resulting strong overshoots put more burdens on the pressure sensors.

3.8. Behavior of the exposed sensors

The previous sections show that shielding the sensor involves some negative drawbacks onto the measurement itself. The cavity and the borehole connecting it to the ambience both affect the signal rise time and involve overshoots and oscillations. Therefore, two sensor holders without protective housing (as shown in Fig. 28) are finally examined.

Fig. 29 summarizes the pressure signals measured with exposed-front blunt and conical holder geometries at different flow conditions. With the absence of boreholes and cavities in front of the sensors, all signals exhibit one pronounced overshoot and settle down rapidly without preceding oscillations. It is noteworthy, however, that the overshoot of the blunt holders is much stronger, but rests to the correct value, while the conical housing gives a constant pressure, which is

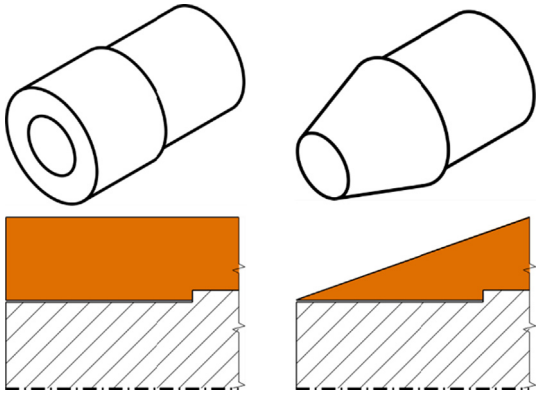

Fig. 28. Configuration of blunt and conical holders (orange colored) with sensors (shadowed) exposed to the freestream. (For interpretation of the references to colour in this figure legend, the reader is referred to the web version of this article.)

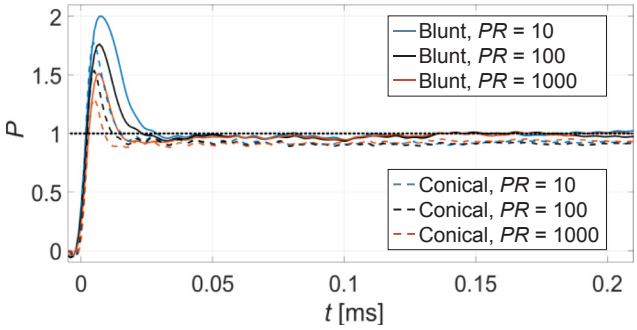

Fig. 29. Normalized pressure signals for exposed sensors in blunt and conical holders at different flow conditions. The black dotted line represents $P = 1$.

about 6% below the reference value.

Maximum Overshoot. For exposed sensors, the incident shock impacts on the entire sensor surface and is subsequently reflected. Hence, overshoots in the range of the previously mentioned theoretical values of 2.06, 1.89 and 1.74 are to be expected. The experimental outcomes for the blunt holders (2.00, 1.76 and 1.51) match the theoretical values well, but the quantitative discrepancy is widened for higher Mach numbers. The reason is simply the higher speed of sound behind the reflected shock and the correspondingly faster adaptation of the pressure field. The maximum overshoots for the conical holders are consequently even lower (1.77, 1.54 and 1.30) since the flow is immediately accelerated to the rim of the sensor surface.

Settling Time. According to the explanation for the maximum overshoot, a steady flow field establishes earlier for a higher speed of sound or smaller geometrical dimensions. It is noteworthy that the settling time can be reduced by a factor of 2 to 3 compared to the blunt sensor housings in Fig. 12.

Steady Value. As already sketched in Fig. 1, the flow in front of a conical sensor decelerates to a stagnation point and subsequently accelerates to the corner of the sensor (or housing) front, where the flow speed reaches Mach number $M = 1$ for transonic flows. Simulations are performed to confirm and illustrate this behavior for both sensor holder geometries (see Fig. 30). In the case of the blunt holder (first row), the pressure in front of the sensor surface (shadowed block) is close to stagnation conditions. Conversely, for the conical holder, the flow acceleration and the associated pressure drop occur at the outer part of the sensor surface. Consequently, the measured signal representing an area-averaged pressure over the sensor surface is lower than the stagnation pressure. This effect of the conical holders on the stagnation pressure measurement agrees very well with the experimentally observed deviation of 6%.

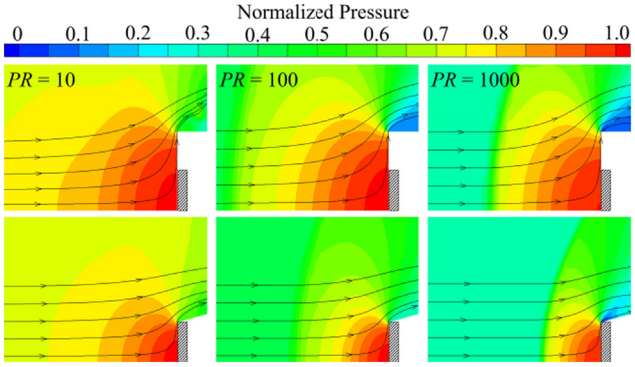

Fig. 30. Pressure contours of the steady-state flow fields around the blunt (top) and conical (bottom) holders at different flow conditions. The shadowed blocks represent the sensor tips.

4. Conclusions

In the present work, the effect of the sensor housing geometries on the stagnation pressure measurement of shock-induced flows is investigated. Housings with two different exterior shapes (blunt and conical) and variations of the internal dimensions (the borehole diameter and the cavity depth) were considered. Each configuration was evaluated at three experimental conditions representing subsonic, transonic and supersonic flows. Influences of other practical factors including the mounting misalignment, the filling with gelatin and the direct exposure of the sensor surface were also assessed. The main points are summarized here:

(1) The blunt housing consistently gives a shorter rise time, a lower maximum overshoot, weaker oscillations and a shorter settling time than the conical housing, mainly due to the built-in advantage of a shorter borehole length.
(2) Decreasing the volume ratio between the cavity and the borehole, either by increasing the borehole diameter or reducing the cavity depth, enhances the strength of the reflected shock at the sensor surface. As a result, the signal rise time is shortened and the overshoot is intensified.
(3) At higher flow Mach numbers, faster wave motions lead to signals oscillating at higher frequencies. The accompanying decrease in the Reynolds number dampens the oscillation amplitudes and shortens the settling time.
(4) The 2° mounting misalignment decreases the pressure measurement by 2–4%. The conical housing is more sensitive to the misalignment than the blunt one.
(5) Filling the housing void with gelatin shortens the rise time, but significantly intensifies the overshoot. This design brings little benefit to the pressure measurement in the current setup.
(6) Experiments with exposed sensors show that the conical sensor holder measures a pressure 6% lower than the stagnation value. Such a deviation is not observed for housings with boreholes and cavities.

To sum up, the blunt housing outperforms the conical one for the stagnation pressure measurement in impulse facilities, by generating less intensely overshooting and more rapidly settled pressure signals. Signal overshoots could be avoided with no sacrifice in the settling time by choosing the borehole diameter and the cavity depth properly. However, the conical housing retains the advantage of less influence on the surrounding flow, and the application of either housing geometry should be case-specific.

Declaration of Competing Interest

There is no financial or personal relationship between authors and other people or organizations that could inappropriately influence or bias the work.

Acknowledgements

The authors acknowledge funding by the European Research Council (ERC) under the European Union's Horizon 2020 research and innovation program (grant agreement No. 667483). The author Z. Wang would like to acknowledge the support from the China Scholarship Council (No. 201606230220).

References

[1] Rex Klopfenstein Jr., Air velocity and flow measurement using a Pitot tube, ISA transactions 37, no. 4 (1998) 257–263.
[2] A.J. Cable, R.N. Cox, The Ludwieg pressure-tube supersonic wind tunnel, Aeronaut. Quart. 14 (2) (1963) 143–157.
[3] Aeronautical Research Council, Bow-shock establishment and stagnation-point pressure measurements for a blunt-nosed body at supersonic speeds, HM Stationery Office, 1965.
[4] J.D. Anderson, Modern Compressible Flow with Historical Perspective, 2003.
[5] Richard Gilman Folsom, Review of the Pitot tube, 1955.
[6] S.H. Chue, Pressure probes for fluid measurement, Progr. Aerospace Sci. 16 (2) (1975) 147–223.
[7] C.R. Gossweiler, On probes and measuring techniques for fast-response flow measurement using piezo-resistive pressure transducers (1995) 0953–0953.
[8] R.M. Lec, Piezoelectric sensors, J. Acoust. Soc. Am. 104 (3) (1998) 1796–1796.
[9] G. Gautschi, Piezoelectric sensors, Piezoelectric Sensorics, Springer, Berlin, Heidelberg, 2002, pp. 73–91.
[10] A.J. Neely, R.J. Stalker, A. Paull, High enthalpy, hypervelocity flows of air and argon in an expansion tube, Aeronaut. J. 95 (946) (1991) 175–186.
[11] A. Paull, R.J. Stalker, Test flow disturbances in an expansion tube, J. Fluid Mech. 245 (1992) 493–521.
[12] Akihiro Sasoh, Yasuyuki Ohnishi, Djameel Ramjaun, Kazuyoshi Takayama, Hirotaka Otsu, Takashi Abe, Effective test time evaluation in high-enthalpy expansion tube, AIAA J. 39 (11) (2001) 2141–2147.
[13] Matthew McGilvray, Peter A. Jacobs, Richard G. Morgan, Rowan J. Gollan, Carolyn M. Jacobs, Helmholtz resonance of pitot pressure measurements in impulsive hypersonic test facilities, AIAA J. 47 (10) (2009) 2430–2439.
[14] M.A. Sutcliffe, R.G. Morgan, The measurement of Pitot pressure in high enthalpy expansion tubes, Measur. Sci. Technol. 12 (3) (2001) 327.
[15] J.W. Naughton, L.N. Cattafesta III, G.S. Settles, Miniature, fast-response five-hole conical probe for supersonic flowfield measurements, AIAA J. 31 (3) (1993) 453–458.
[16] A.R. Porro, Pressure probe designs for dynamic pressure measurements in a supersonic flow field, in: Instrumentation in Aerospace Simulation Facilities, 2001. 19th International Congress on ICIASF 2001, IEEE, 2001, pp. 417–426.
[17] M.K. Bull, A.S.W. Thomas, High frequency wall-pressure fluctuations in turbulent boundary layers, Phys. Fluids 19 (4) (1976) 597–599.
[18] A.D. Tomos, R.A. Leigh, The pressure probe: a versatile tool in plant cell physiology, Annu. Rev. Plant Biol. 50 (1) (1999) 447–472.